Article

Signalling by senescent melanocytes hyperactivates hair growth

https://doi.org/10.1038/s41586-023-06172-8

Received: 11 September 2019

Accepted: 5 May 2023

Published online: 21 June 2023

Open access

Check for updates

Xiaojie Wang[1,2,3]✉, Raul Ramos[1,2,3], Anne Q. Phan[4], Kosuke Yamaga[1,2], Jessica L. Flesher[5], Shan Jiang[1,6], Ji Won Oh[7,8], Suoqin Jin[9,10], Sohail Jahid[5], Chen-Hsiang Kuan[1,2,11,12], Truman Kt Nguyen[1,2], Heidi Y. Liang[1,2], Nitish Udupi Shettigar[1,2,13], Renzhi Hou[1,2,3], Kevin H. Tran[1,2], Andrew Nguyen[1,2], Kimberly N. Vu[1,2], Jennie L. Phung[1,2], Jonard P. Ingal[1,2], Katelyn M. Levitt[1,2], Xiaoling Cao[1,2], Yingzi Liu[1,2,14], Zhili Deng[14], Nobuhiko Taguchi[15], Vanessa M. Scarfone[2], Guangfang Wang[2], Kara Nicole Paolilli[2], Xiaoyang Wang[2], Christian F. Guerrero-Juarez[1,2,3,6,9], Ryan T. Davis[16], Elyse Noelani Greenberg[5], Rolando Ruiz-Vega[5], Priya Vasudeva[5], Rabi Murad[1,6], Lily Halida Putri Widyastuti[2], Hye-Lim Lee[1,2], Kevin J. McElwee[17], Alain-Pierre Gadeau[18], Devon A. Lawson[16], Bogi Andersen[2,3,5,19], Ali Mortazavi[1,6], Zhengquan Yu[20], Qing Nie[1,3,6,9], Takahiro Kunisada[15], Michael Karin[21], Jan Tuckermann[22,23], Jeffrey D. Esko[4], Anand K. Ganesan[5,24], Ji Li[14,25] & Maksim V. Plikus[1,2,3,6,13]✉

Niche signals maintain stem cells in a prolonged quiescence or transiently activate them for proper regeneration[1]. Altering balanced niche signalling can lead to regenerative disorders. Melanocytic skin nevi in human often display excessive hair growth, suggesting hair stem cell hyperactivity. Here, using genetic mouse models of nevi[2,3], we show that dermal clusters of senescent melanocytes drive epithelial hair stem cells to exit quiescence and change their transcriptome and composition, potently enhancing hair renewal. Nevus melanocytes activate a distinct secretome, enriched for signalling factors. Osteopontin, the leading nevus signalling factor, is both necessary and sufficient to induce hair growth. Injection of osteopontin or its genetic overexpression is sufficient to induce robust hair growth in mice, whereas germline and conditional deletions of either osteopontin or CD44, its cognate receptor on epithelial hair cells, rescue enhanced hair growth induced by dermal nevus melanocytes. Osteopontin is overexpressed in human hairy nevi, and it stimulates new growth of human hair follicles. Although broad accumulation of senescent cells, such as upon ageing or genotoxic stress, is detrimental for the regenerative capacity of tissue[4], we show that signalling by senescent cell clusters can potently enhance the activity of adjacent intact stem cells and stimulate tissue renewal. This finding identifies senescent cells and their secretome as an attractive therapeutic target in regenerative disorders.

Stem cells (SCs) are critically required for long-term tissue maintenance and regeneration. To perform their function, SCs remain quiescent and transiently activate only when warranted, a switch that is tightly controlled. Immediate control is exerted by the short-range signalling niche[1]. In addition, activities of thousands of individual SC niches are coordinated by long-range signalling cues from the surrounding tissues[5]. Because long-range signals coordinate activities of many SC niches at once, any changes in them can profoundly alter the overall regenerative potential of an organ. However, which cell types can function as efficient long-range regulators of SCs is poorly understood.

Skin offers a valuable model system for studying these fundamental aspects of SC biology. Skin contains progenitor-rich hair follicles (HFs) that renew in cycles[6]. Each cycle starts with SC activation[7] and requires signalling by the niche, featuring specialized dermal papilla fibroblasts[8]. Although in principle HFs are able to renew cyclically without external signalling inputs, many thousands of HFs physiologically coordinate their hair-making activities for the common goal of proper fur 'manufacturing'[9]. Coordination is achieved via shared signalling between neighbouring HFs[10] and other non-hair skin cell types. The most prominent effects on hair renewal are exerted by skin adipocytes[11] and adipose progenitors[12]. This is possible because HFs and adipose tissue are close to each other and because they use some of the same signalling pathways—WNT, BMP, Hedgehog and PDGF—to regulate their cellular lineages. Innate and adaptive immune cells are also potent modifiers of hair growth dynamics[13,14].

Because cyclic hair renewal is tightly controlled at the level of SC quiescence, naturally occurring conditions of excessive hair growth are rare. Hairy pigmented nevi, both congenital (Fig. 1a,c) and acquired (Fig. 1b), are a type of benign skin lesion in humans that can show prominent hair growth. Despite being well known clinically, the mechanism behind

A list of affiliations appears at the end of the paper.

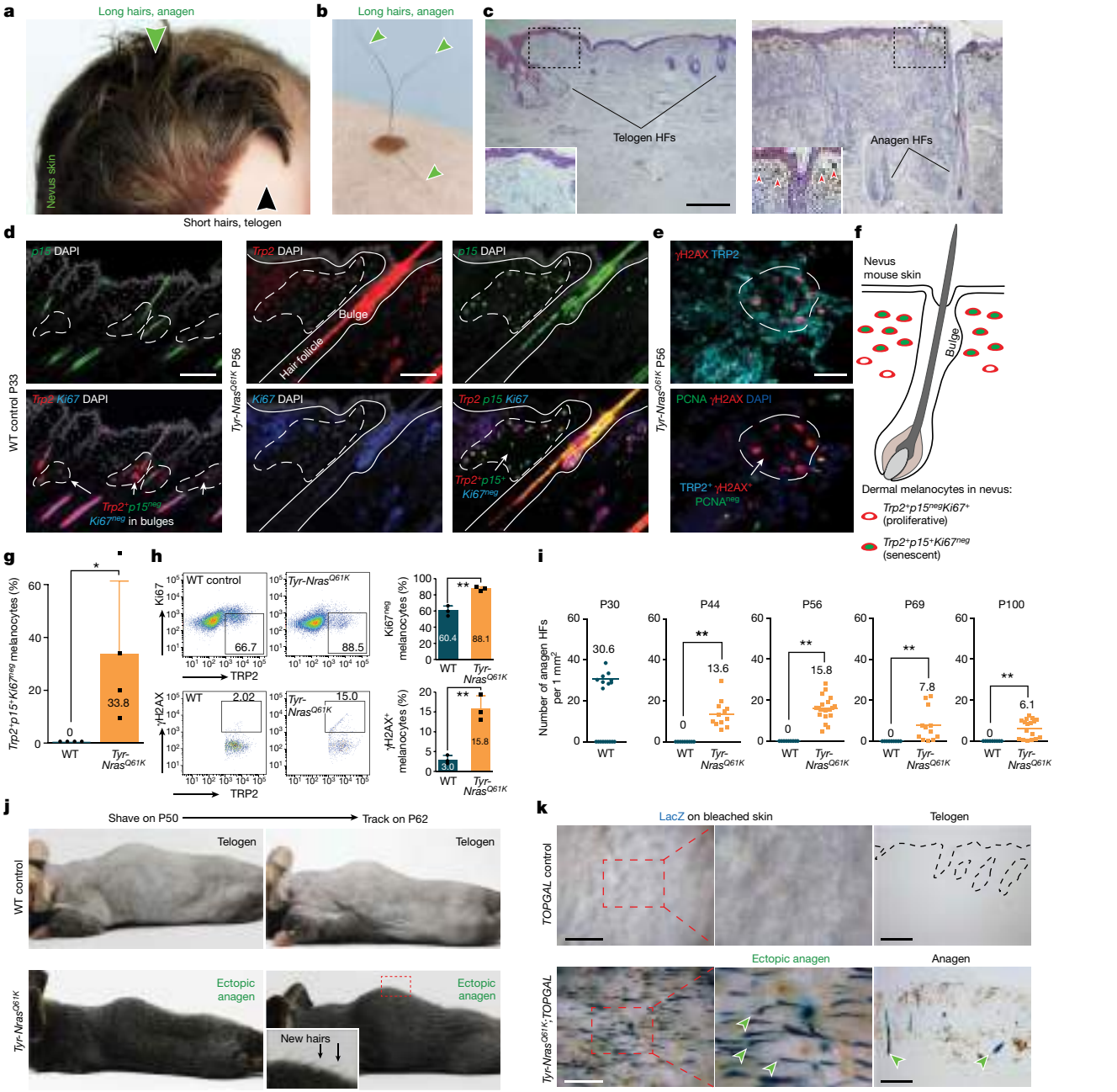

Fig. 1 | Hyperactivation of hair growth in nevus skin. a,**b**, Hair growth (arrowheads) is enhanced within congenital (7-month old; **a**) and acquired (42-year old; **b**) melanocytic nevi in humans. **c**, Facial HFs that commonly remain in telogen in normal skin (left) activate and enter new anagen in nevus skin (right). The red arrowheads mark dermal melanin. **d**,**f**,**g**, Compared with P33 WT anagen skin, P56 *Tyr-Nras*^{Q61K} skin contained clusters of *Trp2*$^{+}$*p15*$^{+}$*Ki67*^{neg} melanocytes in the upper dermis. In **g**, $n = 4$; $P = 0.0455668$. **e**, P56 *Tyr-Nras*^{Q61K} skin contained clusters of TRP2^{+}γH2AX^{+}PCNA^{neg} dermal melanocytes. **h**, Compared with P30 WT anagen skin, P56 *Tyr-Nras*^{Q61K} skin showed significantly increased numbers of TRP2^{+}Ki67^{neg} ($n = 3$; $P = 0.0019135$) and TRP2^{+}γH2AX^{+} melanocytes on cytometry ($n = 3$; $P = 0.0028236$). **i**–**k**, *Tyr-Nras*^{Q61K} mice displayed enhanced hair growth. At all postnatal time points examined (also see Extended Data Fig. 1), *Tyr-Nras*^{Q61K} skin contained many ectopic anagen HFs. Anagen HFs are quantified (**i**). In **i**, $n = 9$ at P30, $n = 12$ ($P = 0.0000108$) at P44, $n = 21$ ($P = 0.0000000000183$) at P56, $n = 12$ ($P = 0.00329$) at P69 and $n = 17$ ($P = 0.0000239$) at P100. In **j**, 12 days after shaving at P50, many new hairs grew in *Tyr-Nras*^{Q61K}, but not in WT mice. In **k**, at P56, *Tyr-Nras*^{Q61K};*TOPGAL* mice, but not control *TOPGAL* mice, showed many lacZ^{+} anagen HFs (arrowheads). In **g**–**i**, *n* refers to biologically independent samples. Data are mean ± s.d. *P* values were calculated using unpaired one-tailed (**g**,**i**) or two-tailed (**h**) Student's *t*-test. $^{*}P \le 0.05$ and $^{**}P \le 0.01$. Scale bars, 20 µm (**e**), 100 µm (**d**), 500 µm (**c**), 1 mm (wholemount; **k**) and 200 µm (histology; **k**). The image in part **a** is reproduced with permission from S. Liber.

excessive hair growth in nevi is not understood. Oncogene mutations, commonly in *Nras* (also known as *Alps4*) or *Braf*, in skin melanocytes induce nevi[15]. Mutant cells first transiently expand but subsequently activate oncogene-induced senescence (OIS)[16], giving rise to a spatially restricted lesion enriched for senescent cells. Once in full senescence, cells express a specialized secretome: the senescence-associated secretory phenotype (SASP)[17]. Several inflammatory cytokines and growth factors are part of the SASP, and their essential signalling roles are being rapidly recognized in normal embryonic development[18], cellular reprogramming[19], injury repair[20] and cancer progression[21,22]. We hypothesized that enhanced hair growth in hairy nevi is driven by activating signalling from dermal clusters of senescent melanocytes to HF SCs.

Senescent cells activate hair growth

First, we asked whether mouse models for melanocytic nevi replicate enhanced hair growth. We studied two established models: constitutive *Tyr-Nras*^{Q61K} mice[2], which model congenital nevi, and inducible *Tyr-CreER*^{T2};*Braf*^{V600E} mice[3], which model acquired nevi. In both models, oncogenes are overexpressed from the *Tyr* enhancer–promoter regulatory region that is highly specific to neural crest-derived melanocytes. Normal hair growth in mice is coordinated: large groups of HFs jointly transition from the resting phase (telogen) to the active growth phase (anagen) and then via the regression phase (catagen) back into telogen[9,11]. This coordination causes HF SCs to spend a large portion of their lifecycle in quiescence, only transiently activated to regenerate new hairs within discrete HF groups. Resting HFs house melanocyte SCs, located in the shared niche with epithelial SCs, whereas growing HFs also contain activated, pigment-producing melanocytes at their base. *Tyr-Nras*^{Q61K} mice, whose dermis but not HFs themselves become populated by senescent melanocytes identified as non-proliferative *p15*$^{+}$ (Fig. 1d,f,g) and non-proliferative γH2AX^{+} melanocytes (Fig. 1e,h), showed dramatically accelerated hair growth, with many ectopic anagen HFs present at any given time ($n = 3$ per time point) (Fig. 1i–k and Extended Data Fig. 1). In control mice, dorsal HFs were in first anagen at postnatal day 15 (P15) (Extended Data Fig. 1a), first telogen by P23 (Extended Data Fig. 1b) and second anagen by P36 (Extended Data Fig. 1c). After that, HFs entered a lengthy second telogen spanning P44–P69 (Extended Data Fig. 1d–g). By contrast, at all time points examined, *Tyr-Nras*^{Q61K} skin contained ectopic anagen HFs (Fig. 1i,j and Extended Data Fig. 1), which were numerous even at P100 (Extended Data Fig. 1h). The ectopic anagen phenotype was especially visible in *Tyr-Nras*^{Q61K};*TOPGAL* mice ($n = 4$), where all anagen HFs strongly activated the *TOPGAL* WNT reporter and stained positive for lacZ (Fig. 1k). Ectopic anagen HF density in *Tyr-Nras*^{Q61K} mice varied between the time points, but on average it was 35.4% relative to synchronous anagen HF density in P30 wild-type (WT) skin (Fig. 1i). We crossed *Tyr-Nras*^{Q61K} mice onto an albino *Tyr*(*C-2J*) background carrying a mutation in the *Tyr* gene. Despite the lack of melanin, albino *Tyr-Nras*^{Q61K} mice displayed ectopic anagen at both P56 and P100 (Extended Data Fig. 1j), indicating that it is not excessive melanogenesis but rather senescent melanocytes that are necessary for the nevus hair phenotype.

Next, we modelled early acquired nevi in *Tyr-CreER*^{T2};*Braf*^{V600E} mice that were treated with tamoxifen either early at P2–P4 or late at P21–P25. Unlike induced control animals, induced mutant mice accumulated clusters of senescent non-proliferative *p15*$^{+}$ (Extended Data Fig. 2a), non-proliferative γH2AX^{+} (Extended Data Fig. 2b,c) and non-proliferative *p16*$^{+}$ (Extended Data Fig. 2d) melanocytes in the dermis adjacent to HFs. Mutant mice induced at P2–P4 displayed prominent ectopic anagen at P44, P56, P69 and P100 ($n = 4$ per time point) (Extended Data Figs. 1k and 4a,b). Across time points, they averaged 35.7% anagen HFs relative to P30 WT skin, which closely phenocopied congenital *Tyr-Nras*^{Q61K} mutants. Likewise, mutant mice treated with tamoxifen at P21–P25 also showed prominent ectopic anagen starting at P56 ($n \geq 3$ per time point) (Extended Data Fig. 4c,d). We also asked whether injection of nevus-derived melanocytes into normal telogen skin would be sufficient to induce ectopic anagen. We sorted tdTomato^{+} melanocyte lineage cells from the skin of congenital *Tyr-Nras*^{Q61K};*Tyr-CreER*^{T2};*tdTomato* (Extended Data Fig. 3a) and acquired *Tyr-CreER*^{T2};*Braf*^{V600E};*tdTomato* mice (Extended Data Fig. 3c). Intradermal injection of sorted cells from both nevus mouse models into telogen skin of *SCID* mice ($n = 4$ each) induced new anagen within 21 days (Extended Data Fig. 3b,e), albeit their continued senescent status at the grafted site was not verified. Yet, by contrast, injection of sorted cells from control *Tyr-CreER*^{T2};*tdTomato* mice isolated during both telogen (P56) and anagen (P33) did not activate new anagen in *SCID* host skin ($n = 4$ each) (Extended Data Fig. 3d,f–i). We also generated senescent β-galactosidase-positive (β-Gal^{+}) melanocytes by exposing primary CD117^{+} newborn mouse melanocytes to H_2O_2 in vitro (Extended Data Fig. 3j–l). Unlike control cultured melanocytes ($n = 7$), DiI-labelled H_2O_2-treated melanocytes induced new anagen in telogen *SCID* skin 21 days after injection ($n = 6$) (Extended Data Fig. 3m–o). We also subcutaneously treated mice with the small-molecule BCL-2 inhibitor ABT-737, which in P56 *Tyr-Nras*^{Q61K} mice, induced prominent apoptosis of melanocytes but did not affect the abundance of HF SCs ($n = 5$) (Extended Data Fig. 5c,d), and in P33 WT mice did not delay normal anagen timing ($n = 7$) (Extended Data Fig. 5e). By contrast, ABT-737 treatment of *Tyr-Nras*^{Q61K} mice significantly reduced ectopic anagen HFs at P56 ($n = 6$) (Extended Data Fig. 5a,b), which we attribute to nevus melanocyte depletion. Next, we studied *K14-Edn3* and *K14-Kitl* mice, which, respectively, showed expansion in dermal and epidermal melanocytes that is not driven by oncogene mutation. Both mouse models showed normal hair cycle progression, with synchronized anagen at P36 ($n = 3$ per model) and synchronized telogen at P56 ($n = 3$ per model) (Extended Data Fig. 5f–i). Last, we induced *Trp53* (also known as *p53*) deletion in melanocytes, which despite being an oncogenic stimulation, did not induce OIS[17], unlike *Nras*^{Q61K} or *Braf*^{V600E} overexpression. Analogous to control mice, HFs in tamoxifen-treated P56 *Tyr-CreER*^{T2};*Trp53*$^{fl/fl}$ mice remained in telogen ($n = 3$) (Extended Data Fig. 5j). Together, our data show that congenital and acquired mouse models for melanocyte OIS reproduce the enhanced hair growth that is clinically observed in human hairy pigmented nevi and that senescent dermal melanocytes, but not normal melanocytes, are necessary and sufficient to hyperactivate HF renewal.

Senescence disrupts SC quiescence

We next asked how bona fide HF bulge SCs are affected by the nevus environment. We profiled their transcriptomes by RNA sequencing (RNA-seq) at P30 and P56, when WT HFs are in anagen and telogen, respectively. Bulge SCs were isolated as GFP^{+}CD34^{+}Pcad^{low} cells both from *K14-H2B-GFP* control mice and *Tyr-Nras*^{Q61K};*K14-H2B-GFP* mutant mice, in which CD34 and Pcad maintain WT expression patterns (Extended Data Fig. 6a,b). RNA-seq revealed prominent gene expression differences between *Tyr-Nras*^{Q61K} and control bulge SCs (Fig. 2a, Extended Data Fig. 6c and Supplementary Table 1). The largest differences were seen at P56, with mutant SCs downregulating and upregulating 973 and 1,159 genes, respectively. Depleted gene ontology categories for mutant SCs included cell cycle block, circadian rhythm, and WNT and JAK–STAT suppression, whereas enriched categories contained cell cycle, cell migration, WNT signalling and skin development (Extended Data Fig. 6d and Supplementary Table 1). These gene ontology signatures indicate that *Tyr-Nras*^{Q61K} bulge SCs lose quiescence. At the gene level, multiple quiescence markers, including *Axin2*, *Bmp2*, *Col17a1*, *Ctgf*, *Fgf18*, *Foxc1*, *Grem1*, *Nfatc1* and *Wif1*, were downregulated in P56 *Tyr-Nras*^{Q61K} SCs (Fig. 2b,c and Supplementary Table 1).

To confirm that the *Tyr-Nras*^{Q61K} bulk RNA-seq signature is not being simply dominated by near-normal activated SCs from ectopic anagen HFs, we compared P56 mutant with P30 anagen and P56 telogen WT bulge cells by single-cell RNA-seq. WT cells from P30 and P56 formed the shared cluster C1 and two phase-specific clusters: anagen-specific C2 and telogen-specific C3 (Fig. 2d–f). Upon marker analysis, C1 cells matched the signature of inner bulge cells, which includes *Chit1*, *Krt6a* and *Krt80*, whereas both C2 and C3 cells matched that of outer bulge bona fide SCs, which includes *Col18a1*, *Krt17*, *Lhx2*, *Tcf7l2* and *Vdr*[23] (Fig. 2h, Extended Data Fig. 6e–j and Supplementary Tables 2 and 3). P56 mutant bulge cells dramatically altered their composition relative to WT cells; some cells contributed to the shared inner bulge cluster C1, others to the WT anagen-specific outer bulge cluster C2, whereas many cells formed two new mutant-specific clusters C4 and C5, which retained a core outer bulge signature (Fig. 2f and Extended Data Fig. 6e). No mutant cells contributed to the WT telogen-specific outer bulge cluster C3, which has a quiescent gene expression signature, including

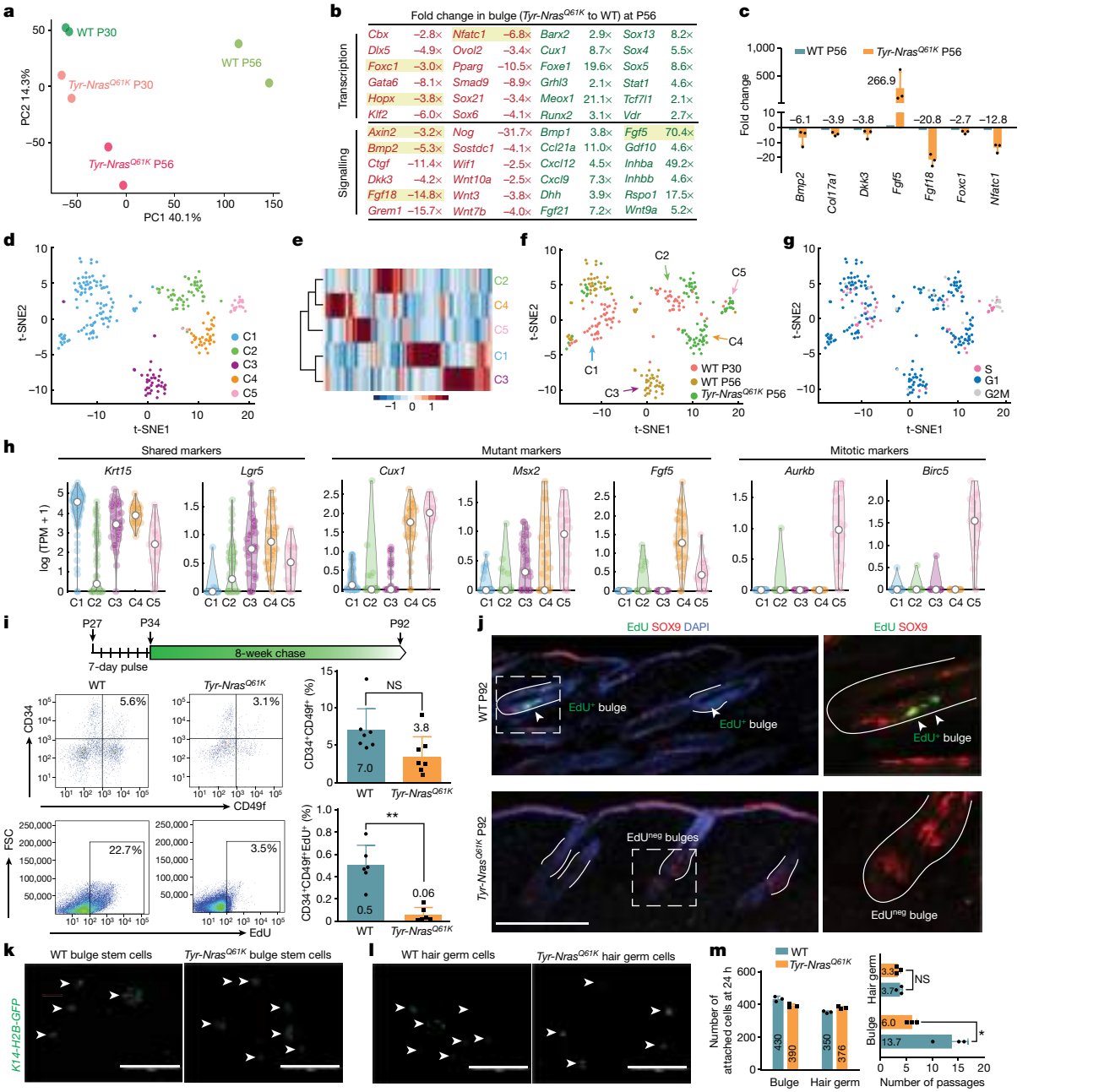

Fig. 2 | Hair SCs within nevus skin lose quiescence. a, On RNA-seq analysis, *Tyr-Nras*^{Q61K} bulge SCs differ from P30 and P56 WT bulge SCs. A principal component analysis plot is shown. See Extended Data Fig. 6. **b**, A list of selected downregulated (red) and upregulated (green) genes at P56 and *Tyr-Nras*^{Q61K} to WT fold change values. **c**, qRT–PCR of selected differentially expressed genes from **a**. $n = 3$. **d**, t-Distributed stochastic neighbour embedding (t-SNE) analysis on single-cell RNA-seq data for P30 and P56 WT and P56 *Tyr-Nras*^{Q61K} bulge SCs. Cells form five clusters: C1 to C5. **e**, Cladogram showing relative cluster similarity. **f**, t-SNE plot colour-coded by sample source. **g**, t-SNE plot colour-coded by inferred cell cycle state. **h**, Violin plots for selected genes. See Extended Data Fig. 6. TPM, transcripts per million. **i**, EdU pulse-chase analysis on bulge SCs. Unlike total numbers of CD34$^+$CD49f$^+$ bulge SCs (top), their EdU$^+$ label-retaining subset reduced significantly in *Tyr-Nras*^{Q61K} versus control mice (bottom). $n = 7$ ($P = 0.061857$) for CD34$^+$CD49f$^+$ SCs and $n = 6$ ($P = 0.0002048$) for CD34$^+$CD49f$^+$EdU$^+$ SCs. See Extended Data Fig. 7. FSC, forward scatter. **j**, Unlike WT, *Tyr-Nras*^{Q61K} HFs from part **i** lacked EdU$^+$SOX9$^+$ bulge SCs (yellow). **k**,**l**, Attachment rates for the *K14-H2B-GFP*$^+$ bulge (**k**) and hair germ (**l**) cells were compatible between WT and *Tyr-Nras*^{Q61K} mice. Arrowheads mark cell colonies. **m**, Compared with WT, *Tyr-Nras*^{Q61K} bulge SCs prominently reduced serial passaging potential, whereas it was unaltered for hair germ progenitor cells. $n = 3$ ($P = 0.5185185$) for hair germ cells and $n = 3$ ($P = 0.0168963$) for bulge cells. In **c**,**i**,**m**, *n* refers to independent experiments. *P* values were calculated using unpaired two-tailed Student's *t*-test. Not significant (NS), $P \geq 0.05$, $^*P \leq 0.05$ and $^{**}P \leq 0.01$. Scale bars, 100 µm (**j**) and 1 mm (**k**,**l**).

Bmp2, *Col17a1*, *Ctgf*, *Grem1*, *Nfatc1*, *Tgm5* and *Wif1* (Extended Data Fig. 6f). Loss of quiescence by mutant-specific outer bulge SCs was further evident from inferred cell cycle analysis: C5 cells were exclusively in S and G2/M phases (Fig. 2g) with prominently upregulated mitotic markers (Fig. 2h and Supplementary Table 3). Given that *Tyr-Nras*^{Q61K} skin contains a mixture of anagen and telogen HFs, the disappearance of WT telogen-specific C3 outer bulge cells supports the loss of quiescence by mutant telogen SCs. Outer bulge marker similarities between clusters C2 to C5 suggest that in the presence of nevus melanocytes, normally quiescent telogen SCs transition to a uniquely activated state.

Next, we confirmed loss of quiescence in functional assays. For pulse and pulse-chase experiments, which measure the cell cycle status of

cells, mice were treated with EdU between P27 and P34, when WT HFs are in anagen and their SCs proliferate. Four hours after the EdU pulse, *Tyr-Nras*^{Q61K} mice displayed bulge SC labelling efficiency that was compatible with WT SCs (Extended Data Fig. 7a,b). However, in a pulse-chase assay, there was a prominent loss of EdU-retaining SCs in *Tyr-Nras*^{Q61K} mice as noted upon analysis at P92 (n = 4 per genotype) (Fig. 2i,j). We then performed a clonogenic assay, which measures long-term proliferative potential by cultured cells and identifies SCs on the basis of them being able to form large clones over many serial passages. We show that the attachment ability of *Tyr-Nras*^{Q61K} bulge SCs was similar to that of WT SCs, but their serial passaging potential was compromised; mutant SCs supported 6 passages (n = 3) compared with 13.7 passages for WT SCs (n = 3) (Fig. 2k,m). A decrease in passaging potential by bulge SCs indicates their faster proliferative exhaustion, a likely consequence of their long-term hyperproliferative status in vivo before culture. Attachment rates and passaging potential, however, did not differ between mutant (n = 3) and WT mice for hair germ cells, a short-lasting population of epithelial progenitors in telogen HFs (n = 3) (Fig. 2l,m).

Osteopontin stimulates hair growth

Next, we asked which signalling factors are expressed by nevus melanocytes. We isolated the melanocyte lineage as tdTomato$^+$ cells from the tamoxifen-induced *Tyr-Nras*^{Q61K};*Tyr-CreER*^{T2};*tdTomato* mutant and *Tyr-CreER*^{T2};*tdTomato* control skin. P56 mutant cells were compared with both P30 anagen and P56 telogen WT cells on bulk RNA-seq (Extended Data Fig. 7c,d). This strategy identified 598 mutant-specific upregulated genes, and also excluded genes regulated as part of the normal hair cycle. Mutant-specific genes were enriched for gene ontology terms, including ageing, WNT suppression, cell cycle block and mitotic division (Extended Data Fig. 7f and Supplementary Table 4). Consistent with dermal clusters of mutant melanocytes undergoing OIS, they upregulated tumour suppressors *Cdkn2b* (also known as *p15*), *Lzts1*, as well as *Cdkn3*, *H2afx* and the mitosis-associated genes *Aurka/b*, *Cdca3/8*, *Cdc20/25c*, *Cenpa*, *Mad2l1*, *Ncaph*, *Knstrn*, *Plk1*, *Psrc1* and *Reep4* (Extended Data Fig. 7g,i). Upregulation of mitosis-associated genes is consistent with the fact that oncogene-stimulated melanocytes enter OIS via a mitotic arrest pathway, rather that via G0 phase[24]. Focusing on the secretome, we identified 27 signalling factors specifically upregulated in nevus melanocytes, including the BMP members *Bmp4* and *Fstl1*, the WNT members *Frzb*, *Wif1* and *Wisp1*, the IGF regulators *Igfbp2/4/7*, as well as *Dhh*, *Fgf7*, *Spp1* (also known as osteopontin) and *Tnf* (Extended Data Fig. 7e). Of note, 68% of the secretome genes enriched in *BRAF*^{V600E}-induced human senescent melanocytes in vitro[2] and 71% of the core in vitro SASP factors[17] were represented in the transcriptome of P56 *Tyr-Nras*^{Q61K} melanocytes (Extended Data Fig. 7h).

Spp1 was one of the topmost upregulated signalling transcripts in nevus melanocytes on RNA-seq. We confirmed this change at the protein level in sorted melanocytes from both the congenital and the acquired nevus mouse models. On cytometry, SPP1 levels were significantly increased in melanocytes from P56 *Tyr-Nras*^{Q61K} mice (n = 3) (Fig. 3a) and from tamoxifen-induced *Tyr-CreER*^{T2};*Braf*^{V600E} mice relative to control melanocytes at five time points between P44 and P100 (n = 3 each) (Fig. 3d and Extended Data Fig. 4f–i). Significantly increased SPP1 levels in P56 *Tyr-Nras*^{Q61K} and in P69 *Tyr-CreER*^{T2};*Braf*^{V600E} melanocytes were confirmed by western blot (n = 3 each) (Fig. 3c,f). Significant increase in SPP1 secretion was observed by ELISA on day 5 cultures of primary melanocytes sorted from P56 *Tyr-Nras*^{Q61K} mice (n = 3) (Fig. 3b) and from *Tyr-CreER*^{T2};*Braf*^{V600E} mice at four time points between P56 and P100 relative to control melanocyte cultures (n = 3 each) (Fig. 3e and Extended Data Fig. 4e). On staining, clusters of *Trp2*$^+$*Spp1*$^+$ melanocytes were observed in the upper dermis adjacent to bulge regions of HFs only in nevus mice, both congenital (Fig. 3g) and acquired (Extended Data Fig. 4l), but not in control mice. Consistent with published gene expression analyses[25], lacZ staining in *Spp1*$^{+/-}$ mice (which carry β-Gal knock-in) shows that *Spp1* expression in normal skin at homeostasis is very restricted, largely limited to dermal papilla fibroblasts of HFs (Extended Data Fig. 8a–c). Together, the above data support that SPP1 is an upregulated signalling factor in dermal clusters of nevus melanocytes.

Next, we asked whether SPP1 has a functional role in hairy nevus phenotype and whether it is sufficient to induce new hair growth. Using *Tyr-Nras*^{Q61K};*Spp1*$^{-/-}$ mice, we showed that a germline loss-of-function mutation in *Spp1* is sufficient to rescue hair cycle quiescence in congenital nevus skin. Compared with *Tyr-Nras*^{Q61K} mice, whose HFs start cycling ectopically already at P23 (Extended Data Fig. 1b), ectopic anagen in *Tyr-Nras*^{Q61K};*Spp1*$^{-/-}$ mice is largely prevented (n = 6 per time point) (Fig. 3h and Extended Data Fig. 8d–g). We also generated *Tyr-CreER*^{T2};*Braf*^{V600E};*Spp1*$^{fl/fl}$ mice, in which tamoxifen treatment induces a conditional *Spp1* loss-of-function mutation in melanocytes along with oncogenic BRAF stimulation. We showed that melanocyte-specific *Spp1* deletion largely prevented ectopic hair cycle in P62 *Spp1*-deficient nevus mice compared with *Spp1*-intact nevus control animals (n = 5 each) (Fig. 3i), and that this correlated with a significant, approximately 70%, decrease in SPP1 secretion in primary melanocyte culture by ELISA (n = 3) (Fig. 3j). Partial SPP1 loss is attributed to incomplete efficiency of *CreER*-based recombination.

Unlike at homeostasis, SPP1 becomes prominently upregulated in skin wounds, both in wound fibroblasts[26] and wound macrophages[27]. Considering this, we asked whether it mediates wound-induced hair growth phenomenon, when HFs at the wound margin enter premature anagen. Indeed, compared with WT mice (n = 8), *Spp1*$^{-/-}$ mice showed significantly fewer anagen HFs at the margin of 5-mm wounds 11 days post-wounding (n = 7) (Fig. 3k). Ectopic anagen was prominently induced 12 days after intradermal injection of SPP1-soaked beads in WT mice compared with BSA-soaked control beads (n = 5 each) (Fig. 3l). Moreover, premature anagen was activated by P54 in *Tyr-rtTA*;*tetO-Spp1* mice, induced with doxycycline starting from P42. Compared with doxycycline-treated control mice, which remained in telogen, *Tyr-rtTA*;*tetO-Spp1* mice displayed broad anagen activation (n = 3 mice each) (Fig. 3m,n). Therefore, SPP1 is sufficient to induce new hair growth and it mediates hair growth activation in at least two skin states: melanocytic nevus and wound healing.

CD44 mediates the osteopontin effect

SPP1 signals via distinct binding sites to its cognate receptors: β-integrins and CD44 (also known as CSPG8). Of these, CD44 is an established stemness marker in several cancer types, where it promotes proliferation, invasiveness and radio-resistance[28]. SPP1 preferentially binds to alternatively spliced CD44v isoforms, which show enrichment in bulge SCs on RNA-seq (Extended Data Fig. 9a). In response to SPP1, CD44 undergoes proteolytic cleavage by γ-secretase, which releases its nuclear-targeted intracellular domain (CD44-ICD), thus coactivating HIF1A, EPAS1, EP300 and CREBBP to regulate gene expression[28]. *Mmp9*, a direct downstream target of CD44-ICD signalling[29], is one of the top upregulated genes in *Tyr-Nras*^{Q61K} bulge SCs (Extended Data Figs. 6c and 9b) and bulge SCs retain high expression of all γ-secretase subunits as well as CD44-ICD-binding transcriptional factors (Extended Data Fig. 9c,d).

We asked whether CD44 mediates hair growth hyperactivation in the nevus. Consistent with previous single-cell RNA-seq profiling, CD44 is prominently expressed across all epithelial compartments of the HF[27], including in bulge SCs, both in control and *Tyr-Nras*^{Q61K} mice (Fig. 4a and Extended Data Fig. 9e). At the protein level, SPP1 colocalizes with CD44 in bulge SCs in both *Tyr-Nras*^{Q61K} and *Tyr-CreER*^{T2};*Braf*^{V600E} mice (Fig. 4c,d). Next, we asked whether *Cd44* deletion compromises bulge SC abundance and proliferative potential. The percentage of either total CD34$^+$CD49f$^+$ bulge SCs or their EdU-labelled

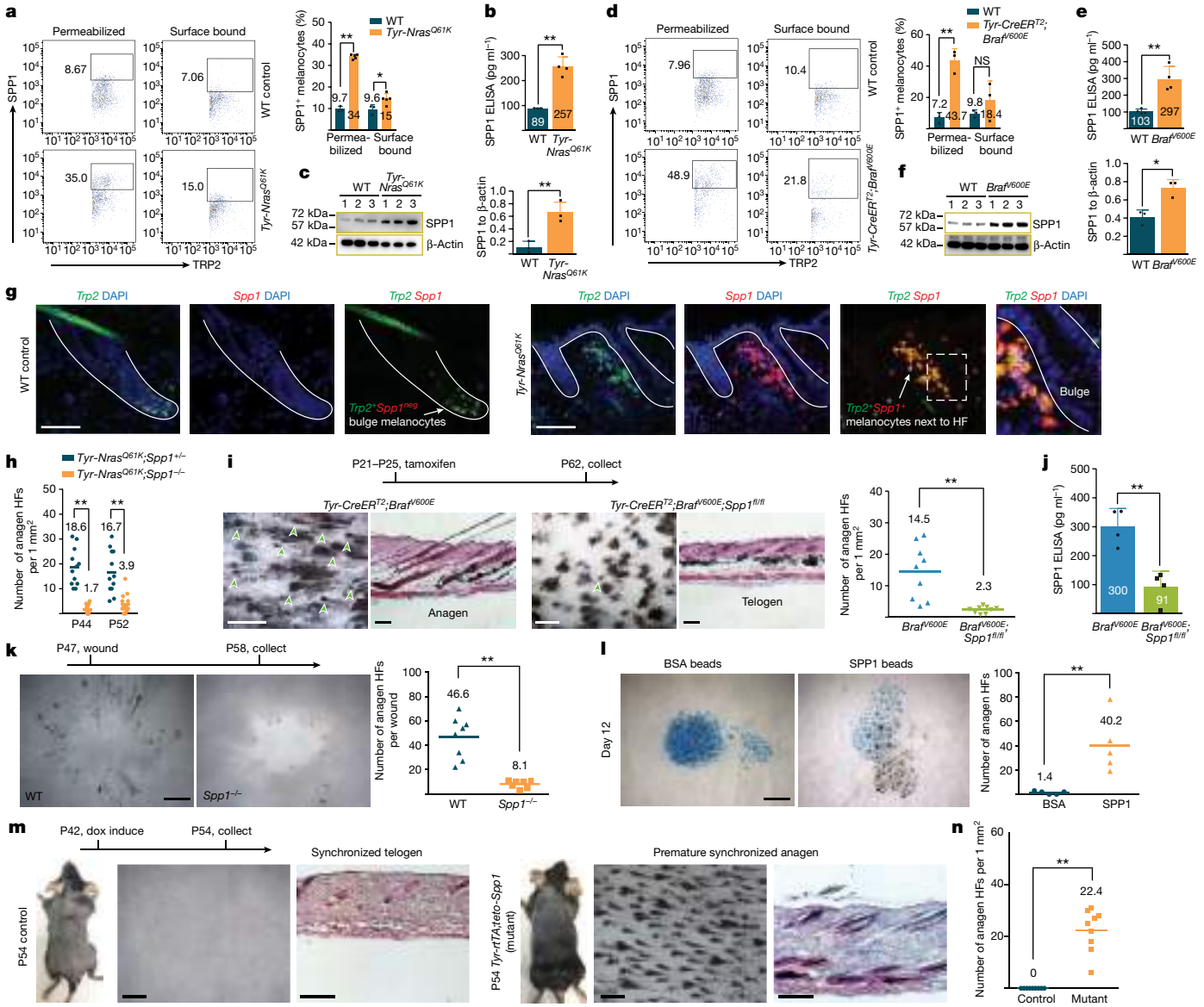

Fig. 3 | Secretome of nevus melanocytes contains SPP1 that promotes hair growth. a,**d**, On cytometry, SPP1 was increased in P56 *Tyr-Nras*^{Q61K} (**a**) and P69 *Tyr-CreER*^{T2};*Braf*^{V600E} (**d**) melanocytes. In **a**, for the permeabilized condition, $n = 3$ in WT and $n = 5$ in *Tyr-Nras*^{Q61K} ($P = 0.000000115$); for the surface-bound condition, $n = 3$ in WT and $n = 5$ in *Tyr-Nras*^{Q61K} ($P = 0.0257$). In **d**, for the permeabilized condition, $n = 3$ ($P = 0.001397$); for the surface-bound condition, $n = 3$ ($P = 0.2888$). See Extended Data Fig. 4. **c**,**f**, On western blot, SPP1 levels were increased in P56 *Tyr-Nras*^{Q61K} (**c**) and P69 *Tyr-CreER*^{T2};*Braf*^{V600E} (**f**) melanocytes. In **c**, $n = 3$; $P = 0.00784$. In **f**, $n = 3$; $P = 0.0109$. Uncropped gels are shown in Supplementary Fig. 1. **b**,**e**, On ELISA, SPP1 levels increased in day 5 cultures of P56 *Tyr-Nras*^{Q61K} (**b**) and P69 *Tyr-CreER*^{T2};*Braf*^{V600E} (**e**) melanocytes. In **b**, $n = 3$ in WT and $n = 4$ in *Tyr-Nras*^{Q61K}; $P = 0.00072$. In **e**, $n = 4$; $P = 0.00224$. See Extended Data Fig. 4e. **g**, Unlike WT, *Tyr-Nras*^{Q61K} skin contained *Trp2*$^{+}$*Spp1*$^{+}$ melanocytes adjacent to HF bulges. **h**, Anagen HF quantification in *Tyr-Nras*^{Q61K};*Spp1*$^{-/-}$ versus *Tyr-Nras*^{Q61K};*Spp1*$^{+/-}$ control mice. At P44, $n = 12$ in control and $n = 14$ in *Tyr-Nras*^{Q61K};*Spp1*$^{-/-}$ ($P = 0.0000000191$); at P56, $n = 12$ in control and $n = 15$ in *Tyr-Nras*^{Q61K};*Spp1*$^{-/-}$ ($P = 0.0000195$). **i**, *Tyr-CreER*^{T2};*Braf*^{V600E};*Spp1*$^{fl/fl}$ mice showed hair cycle quiescence rescue. Representative samples (left) and quantification (right) are displayed. $n = 9$; $P = 0.000731$. Arrowheads mark anagen HFs. **j**, On ELISA, SPP1 levels were reduced in day 5 cultures of *Tyr-CreER*^{T2};*Braf*^{V600E};*Spp1*$^{fl/fl}$ versus *Tyr-CreER*^{T2};*Braf*^{V600E} melanocytes. $n = 4$; $P = 0.00242$. **k**, *Spp1*$^{-/-}$ mice showed reduced wound-induced hair growth. Representative samples (left) and quantification (right) are displayed. $n = 8$ in WT and $n = 7$ in *Spp1*$^{-/-}$; $P = 0.0000575$. **l**, Unlike BSA-soaked beads (blue), SPP1-soaked beads induced anagen in WT skin 12 days after injection. Representative samples (left) and quantification (right) are displayed. $n = 5$; $P = 0.00562$. **m**,**n**, Unlike control, doxycycline (dox)-treated P54 *Tyr-rtTA;tetO-Spp1* mice displayed premature anagen. Representative mice (**m**) and quantification (**n**) are displayed. In **n**, $n = 9$; $P = 0.000000377$. In **b**,**c**,**e**,**f**,**j**, *n* refers to independent experiments. In **a**,**d**,**h**,**i**,**k**,**l**,**n**, *n* refers to biologically independent samples. Data are mean ± s.d. *P* values were calculated using unpaired two-tailed Student's *t*-test. NS, $P \geq 0.05$, $^{*}P \leq 0.05$ and $^{**}P \leq 0.01$. Scale bars, 100 µm (**g**), 200 µm (histology; **i**,**m**) and 500 µm (wholemount; **i**,**k**,**l**,**m**).

subset after 7 days of EdU pulse did not significantly change in germline *Cd44*$^{-/-}$ mutant versus control mice ($n = 3$ each) (Extended Data Fig. 9f,g) as well as in epithelial-specific constitutive *K14-Cre*;*Cd44*$^{fl/fl}$ mutant versus control mice ($n = 3$ each) (Extended Data Fig. 9i,j). Also unchanged was the in vitro colony-forming potential by sorted bulge SCs both from *Cd44*$^{-/-}$ and *K14-Cre*;*Cd44*$^{fl/fl}$ mice versus control animals ($n = 6$ each) (Extended Data Fig. 9h,k). Therefore, loss of CD44 alone does not compromise key bulge SC properties. Next, we asked whether CD44 function is required for HF response to SPP1. Indeed, anagen induction in response to SPP1-soaked beads was significantly suppressed in *Cd44*$^{-/-}$ versus control mice ($n = 5$ each) (Fig. 4e). Likewise, significantly fewer anagen HFs were induced at the wound margin of

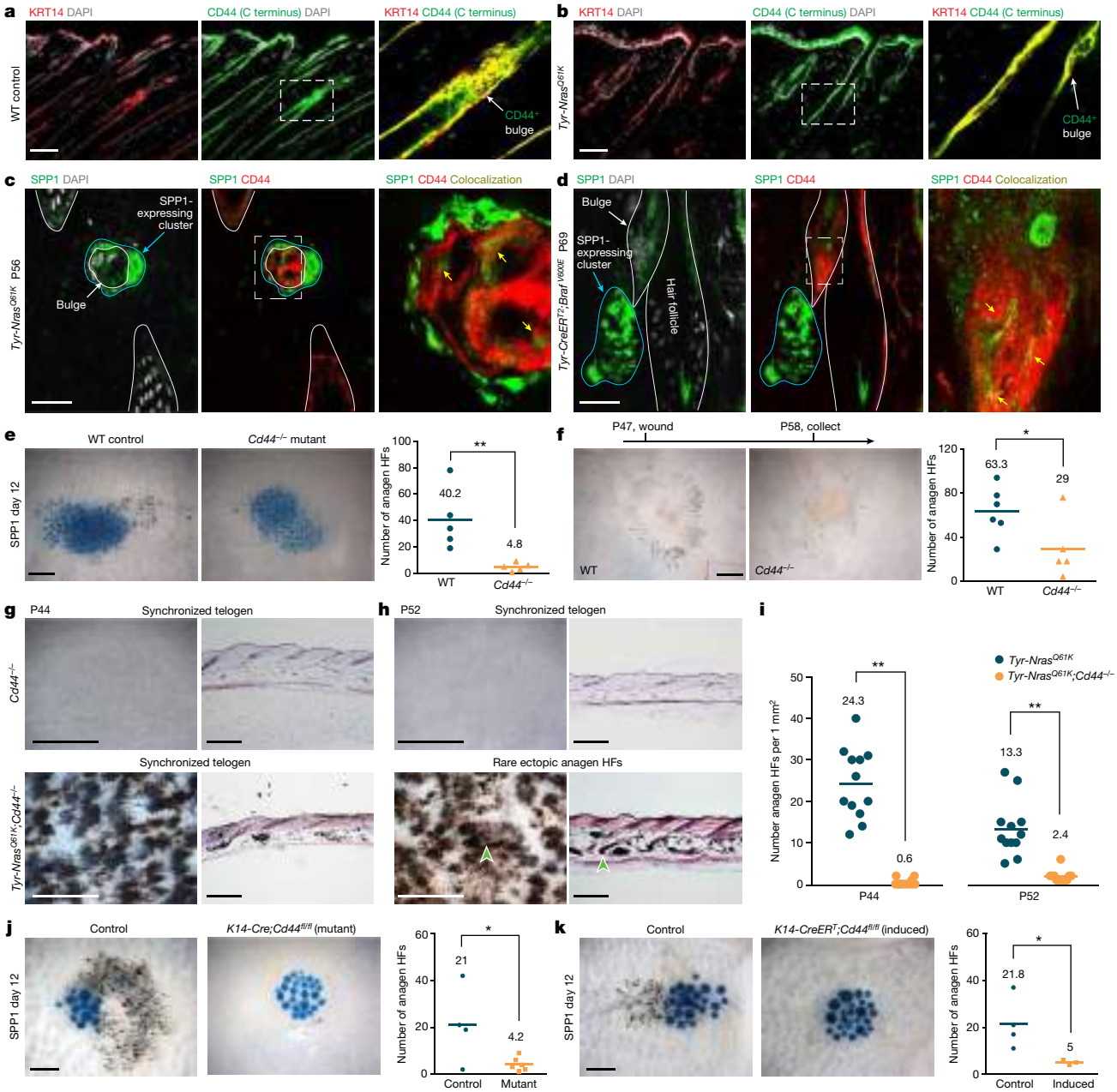

Fig. 4 | Effect of SPP1 on hair growth depends on CD44. a,**b**, Epithelial HF cells in both WT control (**a**) and *Tyr-Nras*^{Q61K} (**b**) mice strongly expressed CD44. Samples were also stained for the epithelial keratin marker KRT14. **c**,**d**, Co-staining for SPP1 and CD44 in *Tyr-Nras*^{Q61K} (**c**) and *Tyr-CreER*^{T2};*Braf*^{V600E} (**d**) skin revealed SPP1^{high} clusters of dermal cells adjacent to CD44^{+} bulge cells with weaker colocalizing SPP1 signal (yellow arrows). **e**, *Cd44*$^{-/-}$ mice showed significantly reduced anagen activation in response to SPP1-soaked beads compared with WT mice. Representative samples (left) and quantification (right) are displayed. $n = 5$; $P = 0.00938$. **f**, *Cd44*$^{-/-}$ mice showed reduced wound-induced hair growth compared with WT mice. Representative samples (left) and quantification (right) are displayed. $n = 6$ in WT and $n = 5$ in *Cd44*$^{-/-}$; $P = 0.0494$. **g**,**h**, *Tyr-Nras*^{Q61K};*CD44*$^{-/-}$ mice lacking *Cd44* showed rescue of hair cycle quiescence. At P44, *Tyr-Nras*^{Q61K};*Cd44*$^{-/-}$ HFs were in coordinated telogen (**g**). Only rare anagen HFs (arrowheads) were present at P52 (**h**). **i**, Quantification of anagen HFs in *Tyr-Nras*^{Q61K} versus *Tyr-Nras*^{Q61K};*Cd44*$^{-/-}$ mice. Double mutants showed reduced ectopic anagen at P44 and P52. At P44, $n = 12$ and $P = 0.00000000249$; at P56, $n = 12$ and $P = 0.0000166$. **j**,**k**, Both constitutive epithelial-specific *K14-Cre*;*Cd44*$^{fl/fl}$ (**j**) and tamoxifen-induced *K14-CreER*^{T};*Cd44*$^{fl/fl}$ (**k**) mice showed significantly reduced anagen activation in response to SPP1-soaked beads compared with control mice. Representative samples (left) and quantification (right) are displayed. In **j**, $n = 4$ in control and $n = 6$ in mutant; $P = 0.0352$. In **k**, $n = 4$ in control and $n = 3$ in induced mutant; $P = 0.0476$. In **e**,**f**,**i**–**k**, *n* refers to biologically independent samples. *P* values are calculated using unpaired two-tailed Student's *t*-test. *$P \le 0.05$ and **$P \le 0.01$. Scale bars, 50 µm (**c**,**d**), 100 µm (**a**,**b**), 200 µm (histology; **g**,**h**), 300 µm (**j**,**k**), 500 µm (**e**,**f**) and 1 mm (wholemount; **g**,**h**).

Cd44$^{-/-}$ mutant ($n = 5$) versus control mice ($n = 6$) (Fig. 4f). Furthermore, *Cd44* deletion in *Tyr-Nras*^{Q61K};*Cd44*$^{-/-}$ mice led to rescue of ectopic hair cycling, phenocopying the effect of *Spp1* deletion in the *Tyr-Nras*^{Q61K} background (Fig. 4g–i and Extended Data Fig. 9l,m). Loss of SPP1 responsiveness in the soaked bead experiment was also phenocopied upon epithelial-specific *Cd44* deletion in *K14-Cre*;*Cd44*$^{fl/fl}$ as well as in tamoxifen-inducible *K14-CreER*^{T};*Cd44*$^{fl/fl}$ mice. Compared with SPP1-treated control mice ($n = 4$ each), the numbers of induced anagen HFs were significantly reduced both in *K14-Cre*;*Cd44*$^{fl/fl}$ ($n = 6$) (Fig. 4j) and in induced *K14-CreER*^{T};*Cd44*$^{fl/fl}$ ($n = 3$) mice (Fig. 4k). Therefore, the hair growth-activating effect of SPP1 in nevus skin requires epithelial CD44 signalling.

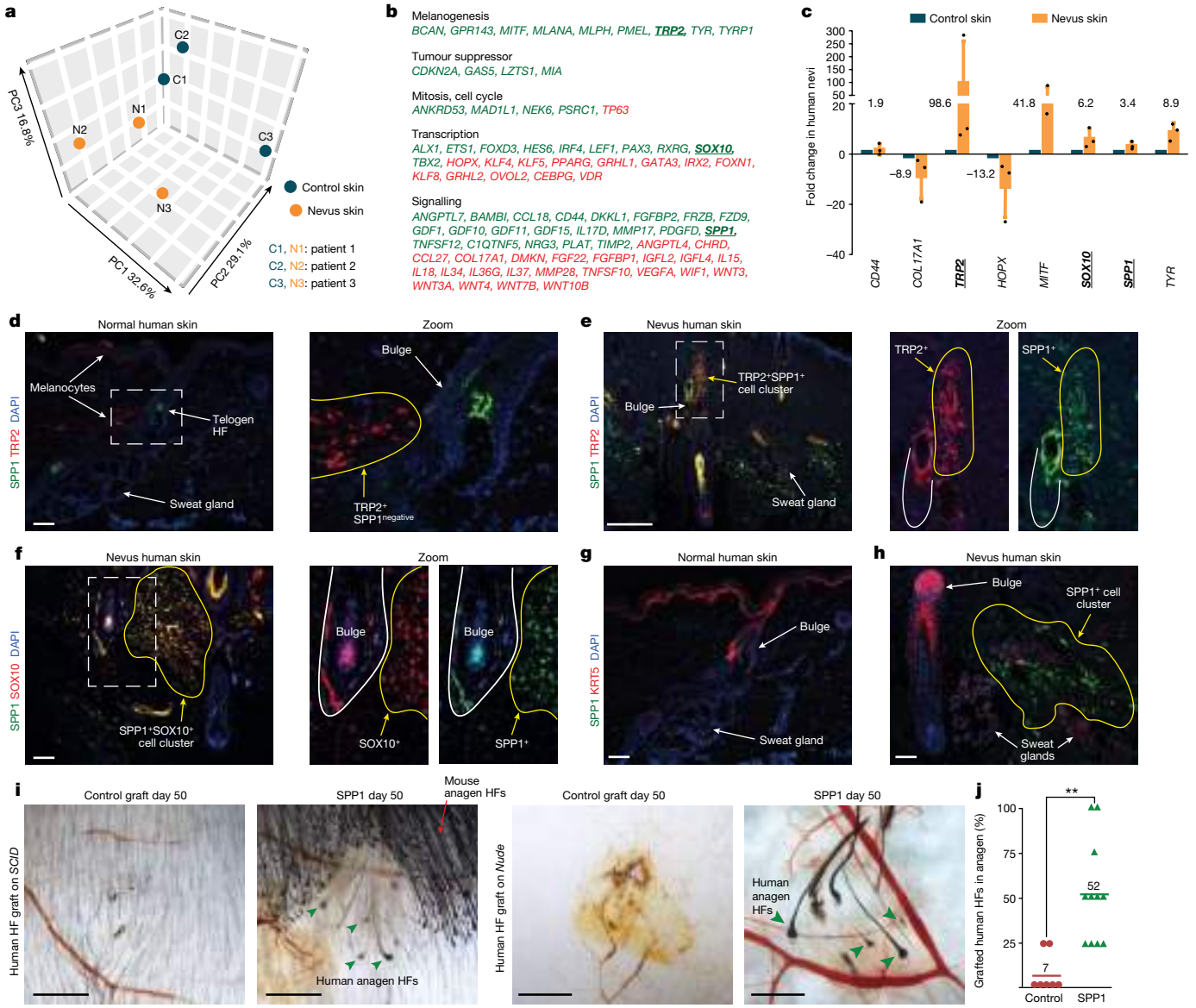

Fig. 5 | Human nevi feature secretome enriched for SPP1. a, Bulk RNA-seq reveals prominent differences between hairy nevi and adjacent normal facial skin in humans. A principal component analysis plot is shown. See Extended Data Fig. 9. **b**, Selected upregulated (by 2× or more; green) and downregulated (by 2× or more; red) differentially expressed genes in nevus versus normal human skin. Bold and underlined genes were validated by qRT-PCR. **c**, qRT–PCR of selected differentially expressed genes from bulk RNA-seq data. $n = 3$. **d**,**e**, SPP1 and TRP2 co-staining. In normal skin, TRP2$^+$ melanocytes did not express SPP1 (**d**), whereas in nevus skin, clusters of TRP2$^+$SPP1$^+$ cells were seen next to HF bulge regions (**e**). **f**, SPP1 and SOX10 co-staining. Nevus skin contained SOX10$^+$SPP1$^+$ cell clusters next to HF bulge regions. **g**,**h**, SPP1 and KRT5 co-staining. Unlike in normal skin (**g**), SPP1$^+$ cell clusters were seen next to HFs in nevus human skin (**h**). **i**,**j**, SPP1 microinjections induced precocious growth by human scalp HFs (arrowheads). Representative samples of human HFs on day 50 post-grafting (**i**) and quantification of human HFs in anagen (**j**) are shown. In **j**, $n = 7$ for control and $n = 11$ for SPP1; $P = 0.00034$. In **c**, n refers to independent experiments. In **j**, n refers to biologically independent samples. P values were calculated using unpaired two-tailed Student's t-test. $^{**}P \leq 0.01$. Scale bars, 100 µm (**d**–**h**) and 1 mm (**i**).

Human hairy nevi upregulate osteopontin

We also examined signalling aspects of congenital hairy nevi in humans. Whole-tissue RNA-seq revealed prominent differences between congenital hairy nevi and adjacent normal facial skin, and patient-to-patient variability (Fig. 5a, Extended Data Fig. 9n,o and Supplementary Table 5). Nevi showed enrichment for the melanogenesis genes *BCAN*, *GPR143*, *MITF*, *MLANA*, *MLPH*, *PMEL*, *SOX10*, *TRP2*, *TYR* and *TYRP1*, and consistent with *Tyr-Nras*^{Q61K} mouse data, they upregulated the tumour suppressor genes *CDKN2A*, *GAS5*, *LZTS1*, *MIA* and the mitotic markers *ANKRD53*, *MAD1L1*, *NEK6* and *PSRC1*, albeit the latter can be contributed by proliferating HF cells. Among secreted factors, nevi upregulated *SPP1*, several TGFβ/BMP members *GDF1/10/11/15* and *BAMBI*, the WNT modulators *DKKL1*, *FRZB*, as well as *CCL18*, *IL17D* and *PDGFD* (Fig. 5b). *SPP1* was among upregulated secretome factors shared between human hairy nevi consistently across patients and *Tyr-Nras*^{Q61K} mouse melanocytes (Extended Data Fig. 9p), which we validated by quantitative PCR with reverse transcription (qRT–PCR) (Fig. 5c) and immunostaining (Fig. 5d–h). SPP1 expression was prominent in dermal clusters of either TRP2$^+$ (Fig. 5e) or SOX10$^+$ melanocytes (Fig. 5f) surrounding bulge regions of HFs. Finally, we tested the hair growth-inducing effect of SPP1 on human scalp HFs in albino *Nude* or pigmented *SCID* host mice[8]. Skin next to telogen HFs were treated with three daily doses of SPP1 or saline. Compared with control ($n = 7$), SPP1 ($n = 11$) accelerated anagen entry

in human HFs, sometime accompanied by anagen entry in mouse HFs (Fig. 5i,j). We conclude that SPP1 is a nevus melanocyte-derived hair growth activator in humans.

Discussion

In this work, we studied how melanocytic skin nevi develop hair overgrowth, which led us to discover that senescent cells can prominently activate tissue-resident SCs and stimulate regeneration. Traditionally, accumulation of senescent cells in tissues is viewed as detrimental to their regenerative potential. This scenario plays out during natural advanced ageing, pathologically accelerated ageing or upon genotoxic exposure[4]. Broad build-up of senescent cells depletes the regenerative capacity of tissues in part via direct elimination of SCs (that is, many SCs become senescent and, thus, non-proliferative) and in part via excessive activation of cytokine-rich secretome (that is, SASP)[17]. SASP factors induce a state akin to low-grade inflammation, which, when persistent, triggers tissue fibrosis. Not surprisingly, systemic depletion of senescent cells in mice delays ageing phenotypes[30], whereas senolytics, drugs that selectively kill senescent cells, have emerged as promising candidate therapeutics for age-related pathologies[31].

However, recent evidence points towards alternative, beneficial effects of senescent cells on tissue growth. Senescent cells form in multiple embryonic tissues, including in the apical ectodermal ridge of the developing limb in mice[18]. Such 'developmental' senescent cells secrete signalling factors thought to instruct growth by surrounding non-senescent embryonic cells. Senescent cells also frequently emerge in non-aged adult tissues upon injury, where SASP factors stimulate enhanced repair. This scenario has been observed in zebrafish after fin amputation[32], in mice following exercise-induced or cardiotoxin-induced skeletal muscle injury[33,34], surgical resection of liver[35] and excisional skin wounding[20]. In tumours, excessive growth by cancer-initiating cells can rely on stimulating paracrine signals from adjacent senescent cells. The latter can form among cancer-associated stromal cells[21,22] or within cancer cell lineage itself, either triggered by an oncogenic mutation (OIS mechanism) or genotoxic anticancer therapy (DNA damage-induced senescence)[36]. The above examples teach that the paracrine component of the cellular senescence program is commonly used as part of the tissue growth-promoting mechanism. The mechanism of hair overgrowth reported by us in skin nevi exemplifies growth-promoting property of senescent cells (Extended Data Fig. 10). In Supplementary Discussion 1, we discuss conditions necessary for the promoting effect of senescent cells on tissue growth and insights offered by the hairy nevus model.

Whether hairy melanocytic nevus is an outlying example of the kind of effects that senescent cells exert on HFs still remains unknown. Indeed, commonly reduced rather than enhanced hair growth is observed in animal models and in people with increased senescent cell burden—advanced age, progeria or exposure to radiation and chemotherapy. Hair overgrowth is also a leading clinical presentation of smooth muscle hamartoma, a congenital or acquired benign nevus-like condition driven by OIS-activating mutations in cutaneous smooth muscle cells[37]. At the same time, nevus sebaceous, where keratinocytes carry OIS-activating mutations, does not present hair overgrowth, but instead features exuberantly enlarged sebaceous glands[38]. We posit that the exact tissue-level consequence of senescence (for example, hair growth versus sebaceous hypertrophy) depends on the exact molecular composition of SASP, which in turn depends on the original lineage of cells that become senescent, the senescence-inducing mechanism and possibly other factors. That SASP composition is probably heterogenous is also strongly supported by molecular data emerging from other recent studies on the senescent cell secretome (reviewed in Supplementary Discussion 2).

SPP1 is the lead SASP factor secreted by senescent dermal melanocytes that potently induces hair growth. SPP1 is also the topmost SASP factor produced by senescent cancer-associated fibroblasts[22], and its signalling via CD44 promotes cancer cell stemness, tumour growth and radio-resistance[28]. We showed that the hair growth-promoting effect of SPP1 also requires an intact CD44 receptor on epithelial cells. Consistently, an SPP1 sequence-based synthetic peptide lacking the CD44-binding site fails to promote epithelial proliferation in cultured human HFs[39]. In this context, our data points to future hair growth-stimulating therapies in which select SASP factors, such as SPP1 or its CD44-binding derivatives, are injected into hair loss-affected skin. In support of this approach are clinical cases reporting hair loss-resistant melanocytic nevi on the scalp of patients with alopecia, including alopecia universalis[40].

Several intriguing questions arise from our study that require future investigation. First, not all melanocytic nevi in people are hairy, probably because they do not satisfy all of the conditions necessary for the growth-promoting effect of senescent cells. In-depth comparison of hairy versus non-hairy human nevi will probably reveal new cellular and molecular diversity of these understudied tissue states. Second, in addition to growing more frequently, hairs in human nevi also become thicker and longer, a property known as terminalization. Because hairs in mice cannot undergo terminalization, future studies on human nevus hairs will probably reveal additional signalling effects of SASP on HF cells, beyond SCs. Third, despite carrying activating oncogene mutations, melanocytes in both *Tyr-Nras*^{Q61K} and Tyr-*CreER*^{T2}; *Braf*^{V600E} mice become senescent in the dermis next to HFs, but not within HFs themselves. This suggests that a distinct signalling microenvironment within HFs can effectively counteract the OIS mechanism. Future studies comparing signals that melanocytes receive from other cells in their dermal versus HF locations will probably identify new senescence-preventing pathways. Last, normally, melanocytes are not critical regulators of HF SCs and hair growth timing (that is, grey hairs still grow robustly). Thus, acquisition of senescence can confer non-niche cells with novel niche-like properties. By the same accord, acquisition of senescence and SASP by 'professional' niche cells (for example, dermal papilla fibroblasts in HFs) may endow them with new regulatory properties. Future works should seek similar effects of cellular senescence on SC functions in other actively renewing organs, such as gut and bone marrow.

In conclusion, our study into the peculiar, yet poorly understood skin condition of hairy nevus led us to identify a distinct regulatory mechanism for adult SCs by tissue-resident senescent cells. These findings have far-reaching implications for advancing our understanding of SC niche regulation and for developing new therapeutic strategies to regenerative disorders.

Online content

Any methods, additional references, Nature Portfolio reporting summaries, source data, extended data, supplementary information, acknowledgements, peer review information; details of author contributions and competing interests; and statements of data and code availability are available at https://doi.org/10.1038/s41586-023-06172-8.

1. Scadden, D. T. Nice neighborhood: emerging concepts of the stem cell niche. *Cell* **157**, 41–50 (2014).
2. Pawlikowski, J. S. et al. Wnt signaling potentiates nevogenesis. *Proc. Natl Acad. Sci. USA* **110**, 16009–16014 (2013).
3. Michaloglou, C. et al. BRAF^{E600}-associated senescence-like cell cycle arrest of human naevi. *Nature* **436**, 720–724 (2005).
4. Campisi, J. Aging, cellular senescence, and cancer. *Annu. Rev. Physiol.* **75**, 685–705 (2013).
5. Hsu, Y. C. & Fuchs, E. A family business: stem cell progeny join the niche to regulate homeostasis. *Nat. Rev. Mol. Cell Biol.* **13**, 103–114 (2012).
6. Muller-Rover, S. et al. A comprehensive guide for the accurate classification of murine hair follicles in distinct hair cycle stages. *J. Invest. Dermatol.* **117**, 3–15 (2001).
7. Cotsarelis, G., Sun, T. T. & Lavker, R. M. Label-retaining cells reside in the bulge area of pilosebaceous unit: implications for follicular stem cells, hair cycle, and skin carcinogenesis. *Cell* **61**, 1329–1337 (1990).

8. Liu, Y. et al. Hedgehog signaling reprograms hair follicle niche fibroblasts to a hyper-activated state. *Dev. Cell* https://doi.org/10.1016/j.devcel.2022.06.005 (2022).
9. Wang, Q. et al. A multi-scale model for hair follicles reveals heterogeneous domains driving rapid spatiotemporal hair growth patterning. *eLife* https://doi.org/10.7554/eLife.22772 (2017).
10. Plikus, M. V. et al. Self-organizing and stochastic behaviors during the regeneration of hair stem cells. *Science* **332**, 586–589 (2011).
11. Plikus, M. V. et al. Cyclic dermal BMP signalling regulates stem cell activation during hair regeneration. *Nature* **451**, 340–344 (2008).
12. Festa, E. et al. Adipocyte lineage cells contribute to the skin stem cell niche to drive hair cycling. *Cell* **146**, 761–771 (2011).
13. Ali, N. et al. Regulatory T cells in skin facilitate epithelial stem cell differentiation. *Cell* **169**, 1119–1129.e11 (2017).
14. Chen, C. C. et al. Organ-level quorum sensing directs regeneration in hair stem cell populations. *Cell* **161**, 277–290 (2015).
15. Roh, M. R., Eliades, P., Gupta, S. & Tsao, H. Genetics of melanocytic nevi. *Pigment Cell Melanoma Res.* **28**, 661–672 (2015).
16. Choi, Y. S. et al. Topical therapy for regression and melanoma prevention of congenital giant nevi. *Cell* **185**, 2071–2085.e12 (2022).
17. Coppe, J. P. et al. Senescence-associated secretory phenotypes reveal cell-nonautonomous functions of oncogenic RAS and the p53 tumor suppressor. *PLoS Biol.* **6**, 2853–2868 (2008).
18. Munoz-Espin, D. et al. Programmed cell senescence during mammalian embryonic development. *Cell* **155**, 1104–1118 (2013).
19. Mosteiro, L. et al. Tissue damage and senescence provide critical signals for cellular reprogramming in vivo. *Science* https://doi.org/10.1126/science.aaf4445 (2016).
20. Demaria, M. et al. An essential role for senescent cells in optimal wound healing through secretion of PDGF-AA. *Dev. Cell* **31**, 722–733 (2014).
21. Wang, T. et al. Senescent carcinoma-associated fibroblasts upregulate IL8 to enhance prometastatic phenotypes. *Mol. Cancer Res.* **15**, 3–14 (2017).
22. Pazolli, E. et al. Senescent stromal-derived osteopontin promotes preneoplastic cell growth. *Cancer Res.* **69**, 1230–1239 (2009).
23. Joost, S. et al. Single-cell transcriptomics reveals that differentiation and spatial signatures shape epidermal and hair follicle heterogeneity. *Cell Syst.* **3**, 221–237.e9 (2016).
24. Dikovskaya, D. et al. Mitotic stress is an integral part of the oncogene-induced senescence program that promotes multinucleation and cell cycle arrest. *Cell Rep.* **12**, 1483–1496 (2015).
25. Rezza, A. et al. Signaling networks among stem cell precursors, transit-amplifying progenitors, and their niche in developing hair follicles. *Cell Rep.* **14**, 3001–3018 (2016).
26. Mori, R., Shaw, T. J. & Martin, P. Molecular mechanisms linking wound inflammation and fibrosis: knockdown of osteopontin leads to rapid repair and reduced scarring. *J. Exp. Med.* **205**, 43–51 (2008).
27. Joost, S. et al. Single-cell transcriptomics of traced epidermal and hair follicle stem cells reveals rapid adaptations during wound healing. *Cell Rep.* **25**, 585–597.e7 (2018).
28. Pietras, A. et al. Osteopontin–CD44 signaling in the glioma perivascular niche enhances cancer stem cell phenotypes and promotes aggressive tumor growth. *Cell Stem Cell* **14**, 357–369 (2014).
29. Miletti-Gonzalez, K. E. et al. Identification of function for CD44 intracytoplasmic domain (CD44-ICD): modulation of matrix metalloproteinase 9 (MMP-9) transcription via novel promoter response element. *J. Biol. Chem.* **287**, 18995–19007 (2012).
30. Baker, D. J. et al. Clearance of p16^{Ink4a}-positive senescent cells delays ageing-associated disorders. *Nature* **479**, 232–236 (2011).
31. Robbins, P. D. et al. Senolytic drugs: reducing senescent cell viability to extend health span. *Annu. Rev. Pharmacol. Toxicol.* **61**, 779–803 (2021).
32. Da Silva-Alvarez, S. et al. Cell senescence contributes to tissue regeneration in zebrafish. *Aging Cell* **19**, e13052 (2020).
33. Young, L. V. et al. Muscle injury induces a transient senescence-like state that is required for myofiber growth during muscle regeneration. *FASEB J.* **36**, e22587 (2022).
34. Saito, Y., Chikenji, T. S., Matsumura, T., Nakano, M. & Fujimiya, M. Exercise enhances skeletal muscle regeneration by promoting senescence in fibro-adipogenic progenitors. *Nat. Commun.* **11**, 889 (2020).
35. Cheng, N., Kim, K. H. & Lau, L. F. Senescent hepatic stellate cells promote liver regeneration through IL-6 and ligands of CXCR2. *JCI Insight* https://doi.org/10.1172/jci.insight.158207 (2022).
36. Lee, S. & Schmitt, C. A. The dynamic nature of senescence in cancer. *Nat. Cell Biol.* **21**, 94–101 (2019).
37. Adulkar, S. A., Dongre, A. M., Thatte, S. S. & Khopkar, U. S. Acquired smooth muscle hamartoma. *Indian J. Dermatol. Venereol. Leprol.* **80**, 483 (2014).
38. Groesser, L. et al. Postzygotic HRAS and KRAS mutations cause nevus sebaceous and Schimmelpenning syndrome. *Nat. Genet.* **44**, 783–787 (2012).
39. Alam, M. et al. An osteopontin-derived peptide inhibits human hair growth at least in part by decreasing FGF7 production in outer root sheath keratinocytes. *Br. J. Dermatol.* https://doi.org/10.1111/bjd.18479 (2019).
40. Yamamoto, T., Okabe, H. & Hoshi, M. Alopecia totalis sparing congenital melanocytic nevus: Renbök phenomenon. *Dermatol. Sin.* **37**, 176–177 (2019).

[1]Department of Developmental and Cell Biology, University of California, Irvine, CA, USA. [2]Sue and Bill Gross Stem Cell Research Center, University of California, Irvine, CA, USA. [3]NSF-Simons Center for Multiscale Cell Fate Research, University of California, Irvine, CA, USA. [4]Glycobiology Research and Training Center, Department of Cellular and Molecular Medicine, University of California, San Diego, La Jolla, CA, USA. [5]Department of Biological Chemistry, University of California, Irvine, CA, USA. [6]Center for Complex Biological Systems, University of California, Irvine, CA, USA. [7]Department of Anatomy, Yonsei University College of Medicine, Seoul, Korea. [8]Department of Anatomy and Hair Transplantation Center, Kyungpook National University and Hospital, Daegu, Korea. [9]Department of Mathematics, University of California, Irvine, CA, USA. [10]School of Mathematics and Statistics, Wuhan University, Wuhan, China. [11]Division of Plastic Surgery, Department of Surgery, National Taiwan University Hospital, Taipei, Taiwan. [12]Research Center for Developmental Biology and Regenerative Medicine, National Taiwan University, Taipei, Taiwan. [13]Amplifica Holdings Group, Inc., San Diego, CA, USA. [14]Department of Dermatology, Xiangya Hospital, Central South University, Changsha, China. [15]Department of Tissue and Organ Development, Regeneration and Advanced Medical Science, Gifu University Graduate School of Medicine, Gifu, Japan. [16]Department of Physiology and Biophysics, University of California, Irvine, CA, USA. [17]Centre for Skin Sciences, University of Bradford, Bradford, UK. [18]University of Bordeaux, INSERM U1034, Adaptation cardiovasculaire à l'ischémie, Pessac, France. [19]Department of Medicine, University of California, Irvine, CA, USA. [20]State Key Laboratory of Farm Animal Biotech Breeding, College of Biological Sciences, China Agricultural University, Beijing, China. [21]Laboratory of Gene Regulation and Signal Transduction, Departments of Pharmacology and Pathology, University of California San Diego, School of Medicine, La Jolla, CA, USA. [22]Institute for Comparative Molecular Endocrinology (CME), University of Ulm, Helmholtzstrasse 8/1, Ulm, Germany. [23]Leibniz Institute on Aging-Fritz Lipmann Institute, Beutenbergstrasse 11, Jena, Germany. [24]Department of Dermatology, University of California, Irvine, CA, USA. [25]Hunan Key Laboratory of Aging Biology, Xiangya Hospital, Central South University, Changsha, China. ✉e-mail: xiaojiw2@uci.edu; plikus@uci.edu